

Graph Attention-Based Symmetry Constraint Extraction for Analog Circuits

Qi Xu, Lijie Wang, Jing Wang, Lin Cheng, Song Chen, Yi Kang

Abstract—In recent years, analog circuits have received extensive attention and are widely used in many emerging applications. The high demand for analog circuits necessitates shorter circuit design cycles. To achieve the desired performance and specifications, various geometrical symmetry constraints must be carefully considered during the analog layout process. However, the manual labeling of these constraints by experienced analog engineers is a laborious and time-consuming process. To handle the costly runtime issue, we propose a graph-based learning framework to automatically extract symmetric constraints in analog circuit layout. The proposed framework leverages the connection characteristics of circuits and the devices' information to learn the general rules of symmetric constraints, which effectively facilitates the extraction of device-level constraints on circuit netlists. The experimental results demonstrate that compared to state-of-the-art symmetric constraint detection approaches, our framework achieves higher accuracy and F₁-score.

I. INTRODUCTION

THE demands for analog integrated circuits (ICs) are increasing rapidly in various fields, such as consumer electronics, medical electronics, smart cars, and other emerging applications. The growing demand for analog ICs necessitates an expedited design process. However, despite some progress in electronic design automation (EDA) tools for analog ICs [1], [2], they still encounter challenges in meeting design requirements during the time-consuming and laborious layout process. To ensure optimal functionality and performance, well-defined constraints (symmetry, matching, etc.) need to be satisfied to guide the layout design. For example, differential topology is often used in analog circuit design to reject common-mode noise and enhance the robustness of the circuit. To prevent the performance degradation of the layout due to the asymmetry of these topological devices, it is necessary to annotate the constraints in advance.

Over the past decade, progress on automated analog IC layout design tools has been relatively slow, with many tools relying on the domain knowledge of experienced engineers. As a result, analog IC layout design still remains a highly manual and expensive task, especially in the face of complex and diverse analog circuits with high design flexibility. Researchers have proposed sensitivity analysis-based methods

to detect constraints [3]–[5]. Using circuit simulation and sensitivity analysis, the key devices that impact performance are identified, and then constraint conditions are generated based on these devices. Although the sensitivity analysis-based approaches can automatically identify critical constraints, due to the computational effort and time-consuming simulation of sensitivity analysis, these methods are limited to standard analog circuit modules with a limited number of devices, such as a simple OTA circuit. Moreover, some works [6]–[8] attempt to convert circuit netlists into graphs and search for subgraphs in a designed database to infer the constraint matching for new designs. However, they require a sufficient number of valid and accurate circuits in the database, and thus are not suitable for increasingly complex analog circuits. In addition, by adopting signal flow analysis to convert analog circuits into simple bipartite graphs, symmetric constraints can be extracted through graph isomorphism algorithms, and matching constraints are further identified through primitive cell recognition with signal flow analysis [9]–[12]. Similarly, an S³DET flow is presented to detect system symmetry constraints by leveraging spectral graph analysis and graph centrality [13]. However, these methods strongly rely on the similarity threshold parameters and face generalization challenges.

Recently, Artificial Intelligence (AI) technology has been widely used in analog ICs. For example, AI has enhanced the conventional approach [14] for fault detection in analog circuits [15], [16], thereby improving the reliability of analog ICs. Similarly, AI-related techniques are presented for analog layout placement [17], [18] and the performance prediction of analog circuits [19]. Recently, leveraging AI methods toward automated extraction of layout constraints for analog ICs is emerging as a trend. Kunal *et al.* [20] utilize a graph neural network (GNN) to handle multiple levels of symmetry hierarchies. However, the function of the GNN in the work is only to solve the graph edit distance (GED) to measure graph similarity, ignoring the adjacent topology at the device-level, and thus cannot effectively extract device-level constraints. A simple and effective methodology is developed in [21] for identifying symmetric matching. It first represents device instances and corresponding pins in the circuit as nodes of a circuit graph, and then embeds the types of devices and pins as node features. Through training a GraphSAGE model [22], adjacent information is aggregated into node embeddings, which are adopted to identify whether two nodes are symmetric. Although the approach improves the accuracy of symmetry constraint extraction, it cannot detect the unpaired constraints with more than two devices, which is not

This work was supported by the National Natural Science Foundation of China (NSFC) under grant No. 62141415 and USTC Research Funds of the Double First-Class Initiative under grant No. YD2100002012. (Corresponding authors: Song Chen, Jing Wang.)

Q. Xu, L. Wang, J. Wang, L. Cheng, S. Chen and Y. Kang are with School of Microelectronics, University of Science and Technology of China, Hefei, China. (e-mail: xuqi@ustc.edu.cn, songch@ustc.edu.cn, jw2019@ustc.edu.cn)

reasonable in analog circuits. Chen *et al.* [23] further propose a gated graph neural network (GGNN)-based method leveraging unsupervised learning to detect symmetric constraints in analog ICs. Since the GGNN aggregates neighboring node features with the convolution operation, the final embedding of each node contains information from its neighboring sub-graph. Based on the node embedding, the cosine similarity of the two nodes is computed as a criterion for symmetry. However, the circuit netlist is converted as a heterogeneous directed multigraph, and thus the computation overhead of the GGNN is tremendously high. Furthermore, the adopted edge features only consider the connections of MOSFETs and passive devices, making it challenging to apply to other types of devices. Additionally, a comprehensive summary of recent advancements in constraint extraction is provided in [24]. Besides, integrating GNN with traditional graph-based algorithms achieves the extractions of analog layout constraints at different design levels [25]. Differing from the above approaches of extracting information directly from SPICE netlists, a novel constraint extraction method based on the layout templates is recently proposed in [26]. However, the approach requires a large number of previous high-quality layouts.

To address these issues, we propose a novel graph-based learning framework to automatically extract layout constraints of analog circuits. Since the edges in netlist graph have different pin connections, an edge-augmented graph attention network (EGAT) is proposed to extract the netlist information. Compared with the traditional graph neural network, which focuses on node-level features, the proposed EGAT pays more attention to the interaction with node and edge features. By utilizing graph neural networks, our framework can analyze existing circuits and learn general rules of symmetry constraints, which in turn generalizes to new unseen circuits. Our main contributions are summarized as follows:

- An edge-augmented graph attention network (EGAT)-based learning framework with a new graph representation is proposed to extract the netlist information effectively and measure the similarity of paired devices according to the resulting embeddings.
- Suitable circuit features are designed to realize information interaction with nodes and edges. Meanwhile, an extra 4-dimensional feature is introduced to distinguish differential pairs and current mirrors in analog circuits.
- Several post-processing rules are developed to significantly reduce the false positive rate.
- Experimental results on typical analog circuit datasets demonstrate that the proposed graph learning framework achieves $> 99\%$ accuracy and $> 94\%$ F_1 -score, significantly outperforming signal flow analysis (SFA) approach [1], the GNN-based extraction approach [21], and the unsupervised learning approach [23] by a large margin.

The rest of the paper is organized as follows. Section II gives the preliminaries and formulates the symmetric constraint extraction problem. Section III describes the details of our proposed graph learning framework. Section IV presents

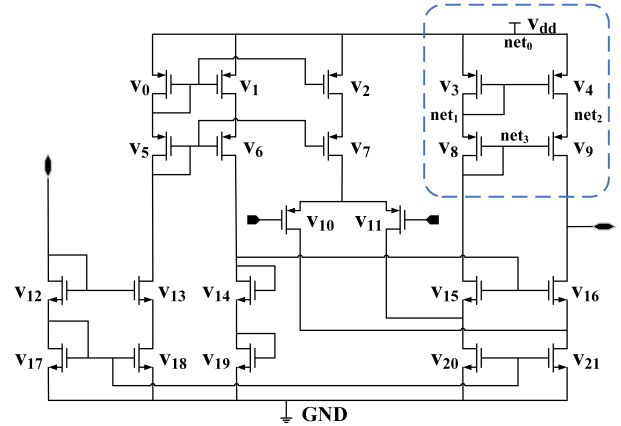


Fig. 1 A typical OTA circuit.

the experimental results, followed by the conclusions in Section V.

II. PRELIMINARIES

In this section, the backgrounds of symmetric constraints in analog circuit layouts and graph neural networks are offered, and then we give the problem formulation.

A. Symmetric Constraints in Analog Circuit Layout

In analog circuit systems, layout symmetry constraints significantly impact circuit performance. Based on the simple fact that the circuit netlist is a graph, we represent the netlist of an analog circuit as a directed graph $G = (V, E)$. V denotes the nodes in the graph, representing circuit devices such as resistors, capacitors, transistors, etc., while E describes the interconnection relationships among devices. For any pairwise combination, we need to detect the symmetrical device pair (v_i, v_j) ($v_i, v_j \in V$), which should be placed symmetrically on the centerline of the layout. Fig. 1 depicts a typical operational transconductance amplifier (OTA) circuit consisting of multiple pairs of symmetrically matched devices, i.e., (v_0, v_1, v_2) , (v_3, v_4) , (v_5, v_6, v_7) , (v_8, v_9) , (v_{10}, v_{11}) , (v_{12}, v_{13}) , (v_{15}, v_{16}) , and $(v_{17}, v_{18}, v_{20}, v_{21})$.

B. Graph Neural Network

In recent years, traditional deep learning methods have achieved great success in extracting features from Euclidean space data. However, there exists a large number of practical application scenarios, where data are generated from non-Euclidean domains and are represented as graphs with complex relationships and interdependency between objects. To handle the complexity of graph data, the graph neural network is developed over the past few years. For example, graph convolutional network (GCN) [27] promotes convolutional operations from traditional data, such as images, to graph data. The main idea is to generate the representation of a node v_i by aggregating its own features with its neighbors' features. The GCN model is the basis of many complex graph neural network structures, including GraphSAGE network [22] and graph generative networks [28]. But different from the GCN

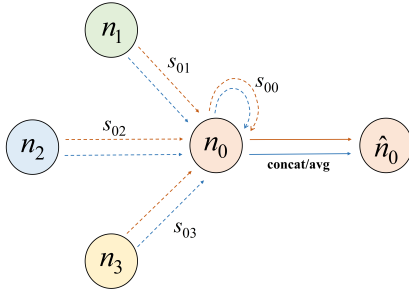


Fig. 2 The illustration of the graph attention mechanism on node 0 with its neighborhood.

model, the GraphSAGE network adopts sampling to achieve a fixed number of neighbors for each node. As a result, the efficiency of information interaction is improved.

In many sequence-based tasks, attention mechanisms have become almost de facto standards, which allow the model to focus on the most relevant parts of the input to make decisions. When an attention mechanism is adopted to calculate a representation of a single sequence, it is considered as a self-attention [29]. Based on the attention mechanism, graph attention network (GAT) [30] is developed to learn the relative weights between two connected nodes. Besides, in order to increase the expressive capability of the GAT model, the multi-head attention is performed for the node embeddings. Fig. 2 depicts the simple aggregation process in the GAT network, where n_i is the feature of node i , and s_{0i} denotes the calculated attention score between node i and node 0. Different arrow colors and styles refer to independent attention computations (multi-head process). Based on the calculated attention score, the feature of the neighboring node i is aggregated in node 0. Then, the aggregated features in each head are concatenated or averaged to achieve the final embedding \hat{n}_0 . But the traditional GAT model only focuses on node-level features and cannot achieve feature interaction between nodes and edges. To tackle the problem, an edge channel is introduced in [31] to explicitly obtain the structural information of a graph. Inspired by [29] and [31], an edge-augmented graph attention network (EGAT)-based learning framework is proposed in this work to pay more attention to the interaction with node and edge features.

C. Problem Formulation

In this work, we formulate the symmetric constraint extraction as a binary classification problem. Several comprehensive measurements are defined to evaluate the detection quality, including true positive rate (TPR), false positive rate (FPR), positive predictive value (PPV), accuracy (ACC), and F_1 -score.

Definition 1 (TPR). *TPR is the number of true positive results divided by the number of all positive results as:*

$$\text{TPR} = \frac{\text{TP}}{\text{TP} + \text{FN}} \quad (1)$$

where TP and FN are the number of the true positive and the false negative results.

Definition 2 (FPR). *FPR is the number of false positive results divided by the number of all negative results as:*

$$\text{FPR} = \frac{\text{FP}}{\text{FP} + \text{TN}} \quad (2)$$

where FP and TN denote the number of the false positive and the true negative results.

Definition 3 (PPV). *PPV is the number of true positive results divided by the number of all predicted positive results as:*

$$\text{PPV} = \frac{\text{TP}}{\text{TP} + \text{FP}} \quad (3)$$

Definition 4 (ACC). *ACC measures the proportion of correctly predicted samples to all samples, representing the overall accuracy of the prediction.*

$$\text{ACC} = \frac{\text{TP} + \text{TN}}{\text{TP} + \text{FP} + \text{TN} + \text{FN}} \quad (4)$$

Definition 5 (F_1 -score). *F_1 -score reflects the balance of the model in positive and negative case classification.*

$$F_1 = \frac{2\text{TP}}{2\text{TP} + \text{FP} + \text{FN}} \quad (5)$$

Based on the above metrics, we define the symmetric constraint extraction problem as follows.

Problem 1 (Symmetric Constraint Extraction). *Given that various analog circuit netlists are labeled with symmetry pairs, the goal is to train a graph learning model to detect the symmetry pairs from the new circuit netlist, yielding higher TPR, PPV, ACC, F_1 -scores, and lower FPR.*

III. PROPOSED GRAPH LEARNING FRAMEWORK

To extract symmetric constraints in analog circuits, we propose a graph learning-based framework as illustrated in Fig. 3, which consists of four main components, namely 1) directed graph representation, 2) input features, 3) edge-augmented graph attention network (EGAT) architecture, and 4) post-processing rules. In the directed graph representation stage, we convert the analog circuit netlist into a graph with bi-directional edges. Then, we utilize partial information of the devices (type, size, etc.) as node features and embed the connection relationship of the devices as edge features, which are then fed to the EGAT network architecture. Next, the proposed EGAT network effectively generates node embeddings, which are adopted to predict the probabilities of symmetry constraint. Finally, in the post-processing stage, several processing rules are designed to rectify the potential symmetry pair errors in EGAT recognition to improve accuracy. The detailed techniques are described below.

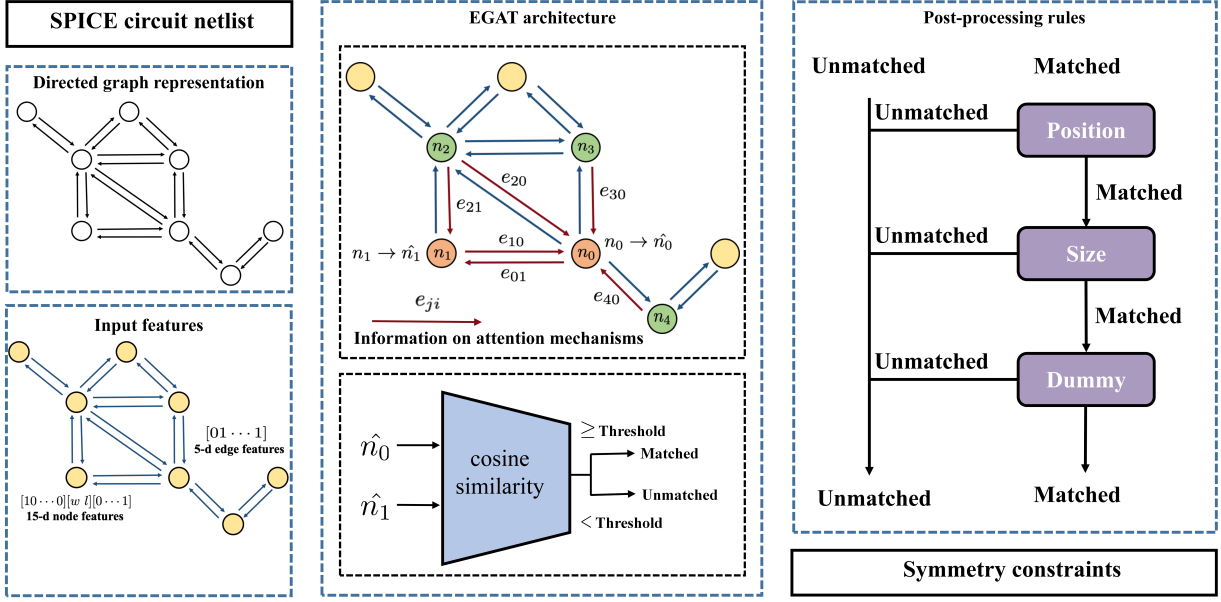


Fig. 3 The diagram of the proposed EGAT-based symmetry constraint extraction framework.

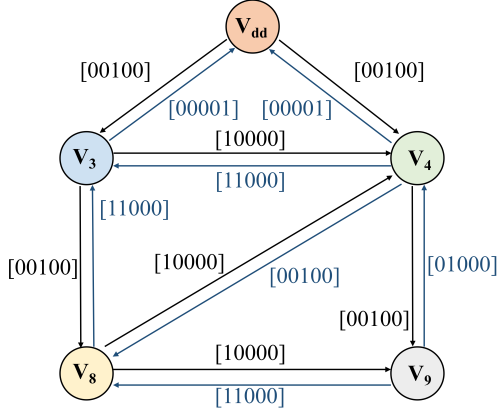


Fig. 4 The directed graph representation for the partial circuit structure in Fig. 1.

A. Directed Graph Representation

In this section, we first explain how to represent a SPICE circuit netlist as a directed graph. For analog circuits, devices and IO ports are nodes of the graph, while the nets connecting devices or IO ports are recognized as edges. For a partial structure of the OTA circuit in Fig. 1 (blue dashed lines), v_3 , v_4 , v_8 , and v_9 are the devices, V_{dd} is the power IO port, and net_0 , net_1 , net_2 , and net_3 refer to the nets. Since different connection directions between nodes indicate varying connection information, bi-directional edges between any two nodes are constructed in the graph. Thus, the number of edges depends on the number of nodes and the circuit's connectivity. The corresponding directed graph representation is depicted in Fig. 4. As illustrated in the graph, node v_3 has bi-directional edges with nodes v_4 , v_8 , and v_{dd} , respectively.

B. Input Features

After the directed graph construction, we define an initial feature vector for each node. Since the size and type of the node are important factors for effectively identifying symmetric constraints, we convert the node type (i.e., NMOS, PMOS, NPN, PNP, diode, resistance, capacitance, inductance, IO) into a unique one-hot representation of a 9-dimensional vector. Note that matched devices should be indeed identical, not just the same type or from the same library. Moreover, the size information of a device is represented as a 2-dimensional vector, where length and width serve as one dimension, respectively. Besides, the influence of fingers is also taken into account. In the circuit design process, when the width of a device is set to w (unit width), and the number of fingers is n_f , the device in the schematic will have a width of w (unit width), but in the SPICE netlist, the device width obtained is $w \cdot n_f$ (total width). Therefore, we need to divide the number of fingers n_f to get the device's unit width w . For instance, if a device has a length and width of $10\mu\text{m}$ with a finger value of 2, the length remains unchanged, while the width needs to be divided by the finger value. As a result, the corresponding 2-dimensional feature is $[10, 5]$. To facilitate neural network training, the 2-dimensional size vector of device nodes is normalized with values between $[0, 1]$, while the IO node's size is set to a default value of -1 .

Due to many differential pairs and current mirrors exist in the analog circuit, and the main difference between them is the connection relation of the gates, an extra 4-dimensional feature is introduced to make the network perceive the connection difference. The detailed description of this 4-dimensional feature is as follows. If the device is not a MOSFET, the feature is configured as $[1, 0, 0, 0]$. For the PMOS (NMOS) device, when its gate port is connected to the gate port of another PMOS (NMOS) device, the feature is set to $[0, 1, 0, 0]$. But if the above condition does not hold and the gate port

of the device is linked to an IO, its feature is adjusted to $[0,0,1,0]$. In all other cases, the feature is designated as $[0,0,0,1]$. Following the specified order above ensures a prioritized assignment, preventing potential ambiguities. For instance, in Fig. 1, although the gate port of NMOS device v_{12} is connected to the IO port, its gate port is also linked to the gate port of NMOS device v_{13} , connections to the gate ports of the MOSFET have higher priority. So the corresponding feature of v_{12} is set to $[0,1,0,0]$. After obtaining the vector representations of three parts, we concatenate them into a 15-dimensional vector as the final node feature.

In addition, a 5-dimensional multi-hot vector is encoded for edges to represent the connection information. The first four dimensions indicate the connections to the gate port, drain port, source port of MOS, and passive device, while the last dimension denotes other possible pin connections (NPN, PNP, etc.). Fig. 4 illustrates the construction process of edge features. The edge connections are as follows: node v_3 is connected to the gate port of node v_4 , the source port of node v_8 , and the power port V_{dd} ; node v_4 is connected to the gate and drain ports of node v_3 , the source ports of nodes v_8 and v_9 , and the power port V_{dd} ; node v_8 is connected to the gate and drain ports of node v_3 , and the gate ports of nodes v_4 and v_9 ; node v_9 is connected to the drain port of node v_4 , and the gate and drain ports of node v_8 . Therefore, based on the constructed graph connections, the feature for the edge from v_3 pointing to v_4 is $[1,0,0,0,0]$, while the feature for the edge from v_4 pointing to v_3 is $[1,1,0,0,0]$. Other edge features are also represented in the graph, with the colors of edges matching their respective features to make the illustration more clear. TABLE I summarizes the initial features and dimensions of nodes and edges, which are concatenated into vector representations and then passed to the downstream graph network.

C. EGAT Architecture

Based on the input node and edge features, the developed EGAT network further extracts the embeddings of nodes and edges. In order to increase the expressive capability of the model, an edge-augmented attention mechanism is performed for each node. Each layer l in the EGAT consists of four calculation processes: layer normalization, attention score calculation, node embedding update, and edge embedding update, as shown in Fig. 5.

Layer Normalization (LN) [32] plays a crucial role in standardizing inputs, avoiding the exploding or vanishing gradients, and accelerating the training process. The calculation process of LN is as follows.

$$\begin{aligned} \mu^l &= \frac{1}{n^l} \sum_{i=1}^{n^l} x_i^l, \quad (\sigma^l)^2 = \frac{1}{n^l} \sum_{i=1}^{n^l} (x_i^l - \mu^l)^2, \\ \hat{x}^l &= \frac{x^l - \mu^l}{\sqrt{(\sigma^l)^2 + \epsilon}}, \quad \text{LN}_{\alpha,\beta}(x^l) = \alpha \odot \hat{x}^l + \beta, \end{aligned} \quad (6)$$

where x^l is the input of the l -th layer, and n^l refers to the number of neurons in the l -th layer. μ^l and σ^l represent the mean and the standard deviation of the input data, respectively.

TABLE I Designed features of nodes and edges in the directed graph representing the analog circuit netlist.

Type	Feature Description	Dimension
Node	One-hot representation for device type	9
	Length and width of device	2
	Connection relationship of gate port	4
Edge	Connection information between pins	5

Besides, ϵ is a small constant, while α and β are learnable parameters with the same dimension as x^l . \odot is the Hadamard product. In this work, we first perform the LN on the initial features as follows.

$$\hat{\mathbf{n}}^l = \text{LN}_{\alpha,\beta}(\mathbf{n}^l), \quad \hat{\mathbf{e}}^l = \text{LN}_{\alpha,\beta}(\mathbf{e}^l), \quad (7)$$

where \mathbf{n}^l and \mathbf{e}^l are the embeddings of all nodes and edges in the l -th layer. As the LN technique enables the model to adapt to various inputs, the model can generalize to new unseen netlists.

Then the multi-head attention mechanism is performed over the learned node representations produced by LN. The attention score of node v_i with its neighbouring node v_j are computed as follows.

$$\begin{aligned} \mathbf{a}_{ij}^l &= \text{reshape}((\mathbf{W}_i^l \hat{\mathbf{n}}_i^l) \odot (\mathbf{W}_j^l \hat{\mathbf{n}}_j^l)) + \mathbf{W}_e^l \hat{\mathbf{e}}_{ij}^l, \\ s_{ij}^l &= \frac{\exp(\mathbf{b}^{l\top} \mathbf{a}_{ij}^l)}{\sum_{j \in \mathcal{N}_i} \exp(\mathbf{b}^{l\top} \mathbf{a}_{ij}^l)}, \end{aligned} \quad (8)$$

where $\hat{\mathbf{n}}_i^l \in \mathbb{R}^{d_n}$, $\hat{\mathbf{n}}_j^l \in \mathbb{R}^{d_n}$ and $\hat{\mathbf{e}}_{ij}^l \in \mathbb{R}^{d_e}$ are the embeddings of node v_i , node v_j and the corresponding edge. $\mathbf{W}_i^l \in \mathbb{R}^{d_n \times d_n}$, $\mathbf{W}_j^l \in \mathbb{R}^{d_n \times d_n}$, $\mathbf{W}_e^l \in \mathbb{R}^{d_e \times d_e}$ and $\mathbf{b}^l \in \mathbb{R}^{d_e}$ denote learning parameters. $\text{reshape}(\cdot)$ refers to the reshape operations. Besides, \mathcal{N}_i represents the neighborhoods of node v_i in the graph. In reality, due to the multi-head attention mechanism, the above calculation is decomposed in multiple heads. The calculated attention score s_{ij}^l indicates the importance of node v_j 's embedding to node v_i .

On the basis of the attention scores, the node embeddings are updated by the weighted average pooling operation. To further enhance the representation ability of the model, we use an MLP to carry out the non-linear transformation of the pooled node embeddings. Besides, the residual connection is performed to facilitate training networks [33]. The final node representation is updated as:

$$\mathbf{n}_i^{l+1} = \text{MLP}_n(\mathbf{n}_i^l + \widetilde{\mathbf{W}}^l \sum_{j \in \mathcal{N}_i} s_{ij}^l \cdot \text{concat}(\mathbf{W}_k^l \hat{\mathbf{n}}_j^l, \widehat{\mathbf{W}}_e^l \hat{\mathbf{e}}_{ij}^l)), \quad (9)$$

where $\mathbf{W}_k^l \in \mathbb{R}^{d_n \times d_n}$, $\widehat{\mathbf{W}}_e^l \in \mathbb{R}^{d_e \times d_e}$ and $\widetilde{\mathbf{W}}^l \in \mathbb{R}^{(d_n+d_e) \times d_n}$ refer to learning weight vectors. $\text{concat}(\cdot)$ represents the concatenation operation. $\text{MLP}_n(\cdot)$ denotes a non-linear transformation with input dimension d_n and output dimension d_n .

Similarly, the edge representation is also updated with a residual connection as follows:

$$\mathbf{e}_{ij}^{l+1} = \text{MLP}_e(\mathbf{e}_{ij}^l + \mathbf{a}_{ij}^l), \quad (10)$$

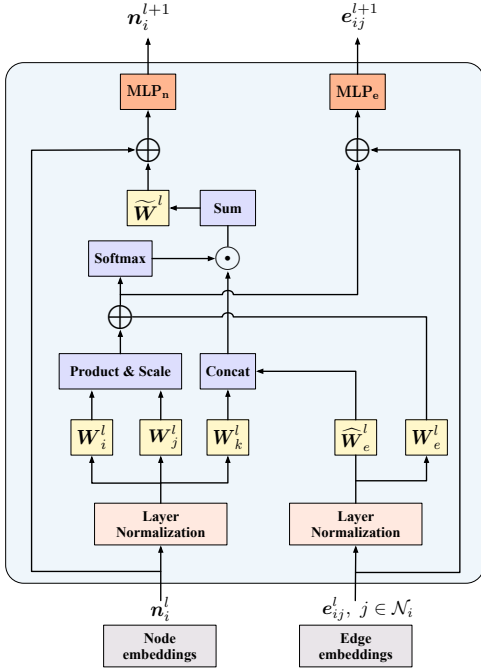


Fig. 5 The architecture of the EGAT network.

where $\text{MLP}_e(\cdot)$ refers to another non-linear transformation with input dimension d_e and output dimension d_e , and a_{ij}^l is the intermediate feature calculated in Equation (8).

As demonstrated above, the proposed EGAT network differs from the traditional attention method in GAT network [30] in that edge features are introduced to calculate attention scores, which are further adopted to update both node and edge features. As a result, the information interactions between nodes and edges are realized. Since the edge features reflect the pin connectivity between nodes, by incorporating the edge feature into the calculation of the attention score, the symmetric matching pairs can be distinguished effectively. Therefore, EGAT makes full use of the characteristics of the netlist graph for the symmetric constraint extraction in analog circuits.

Based on the node embeddings generated by the EGAT architecture, we should provide a predicted similarity score for each candidate symmetry pair (v_i, v_j) ($v_i, v_j \in V$). As the symmetric constraint extraction is formulated as a binary classification problem, labels are annotated in advance, where the symmetric and asymmetric node pairs are labeled as 1 and -1 respectively. To match with the labels, the cosine similarity function is adopted to predict the probabilities of symmetry constraint.

$$\text{similarity} = \frac{\mathbf{n}_i \cdot \mathbf{n}_j}{|\mathbf{n}_i| |\mathbf{n}_j|}, \quad (11)$$

where \mathbf{n}_i and \mathbf{n}_j are the embeddings of nodes v_i and v_j produced by the EGAT.

Due to the utilization of the cosine similarity function, the binary cross-entropy loss [34] originally used to infer results in the range [0,1] is no longer valid. To accommodate this, the logistics loss function is employed for the output label

Algorithm 1 The Pseudo-code of Device Position Calculation

Input: A directed graph G for a circuit.

Output: The position p_n of each device.

```

1:   ▷ Assign weights for edges
2:   for each edge  $e$  in  $G$  do
3:     Get two devices connected by  $e$  as  $d_i$  and  $d_j$ ;
4:     if  $d_i$  and  $d_j$  are passive devices then
5:       Set the weight of  $e$  to 0;
6:     else if  $d_i$  or  $d_j$  is a passive device then
7:       Set the weight of  $e$  to 0.5;
8:     else
9:       Set the weight of  $e$  to 1;
10:    end if
11:  end for
12:  ▷ Find the device position
13:  for each node  $n$  in  $G$  do
14:    if  $n$  is a PMOS then
15:      Calculate the shortest path from power node to  $n$ ;
16:       $p_n$  = the weighted length of the path;
17:    else if  $n$  is a NMOS then
18:      Calculate the shortest path from GND node to  $n$ ;
19:       $p_n$  = the weighted length of the path;
20:    else
21:       $p_n$  = 0.
22:    end if
23:  end for

```

with 1 and -1 as:

$$\text{loss} = \log(1 + e^{-gs}), \quad (12)$$

where gs is the product of the ground truth and the similarity score, which reflects the accuracy and the confidence level of prediction. That is, when $gs \geq 0$, the prediction is correct, and the larger the value, the higher the confidence level. On the contrary, when $gs < 0$, the prediction is incorrect, and the smaller the value, the lower the confidence level.

D. Post-Processing Rules

Although the graph learning framework can annotate the symmetry constraints, a case still exists where asymmetric pairs are identified as symmetry constraints. Thus, we further develop several post-processing rules to reduce the false positive rate (FPR). Note that the developed post-processing rules are only employed to correct the output of the model during the testing (inference) phase.

Firstly, we observe that symmetric device pairs tend to have identical device positions, as defined below.

Definition 6 (Device Position). For each PMOS device, we find the shortest path from the power node to the device. Conversely, for each NMOS device, the shortest path from the GND node to the device is calculated. The weighted length of the shortest path refers to the device position.

Algorithm 1 depicts the process of determining the positions of the devices in an analog circuit. Fig. 6 shows the

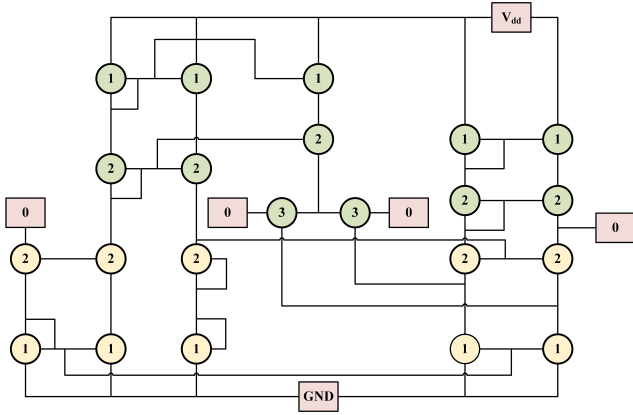


Fig. 6 The illustration of device positions, where the green and yellow circles represent PMOS and NMOS devices and the pink rectangle denotes IO ports.

device positions of the OTA circuit in Fig. 1. It can be seen that symmetric devices exhibit the same device positions.

The second rule is that symmetric pairs must have the same size. Although the designed features of nodes in the neural network contain the type and size information, some device pairs with varying sizes are incorrectly recognized as symmetric pairs after the EGAT recognition. For instance, due to functional requirements in circuit design, devices of the same type but different flavors (models) usually exhibit differences in size. Thus, if the mismatch occurs in the neural network’s output, this post-processing rule will eliminate it. Taking the NMOS as an example, mismatching between low- V_{th} (threshold voltage) NMOS and regular- V_{th} NMOS can be effectively removed by the rule.

In analog circuit schematics, dummies refer to virtual devices without any actual electrical functionality in the circuit design. Instead, they are introduced to meet the requirements of the layout or to be in conjunction with the corresponding devices in the layout. Thus, if a matching pair contains dummy devices, we will eliminate it in the post-processing.

IV. EXPERIMENTAL RESULTS

A. Simulation Setup

The proposed graph learning framework is implemented in Python with the Pytorch library [35], and we execute it on a Linux server with the Intel Xeon Gold 6254 CPU and Nvidia Tesla V100 GPU. The proposed EGAT architecture includes a three-layer network with five attention heads. The threshold for the similarity score calculated in Equation (11) is set to 0.6. That is, if the similarity score of a valid pair is greater than 0.6, the pair will be annotated as a symmetry constraint. Unlike the most commonly used threshold of 0.9 or higher, the low threshold ensures that more symmetric pairs are correctly identified, despite potentially resulting in a higher false alarm rate. But the developed post-processing can effectively eliminate these misidentified pairs. In the experiment, we perform 500 training epoches, with a batch size of 256 for each epoch. The initial learning rate is set to 0.002. Besides, the adaptive moment estimation (Adam)

optimizer [36] is adopted to train the network models. We have open-sourced the codes on GitHub ¹.

B. Dataset Generation

To demonstrate the effectiveness and scalability of our proposed graph learning framework, we conduct comprehensive experiments on real-world analog circuits. Specifically, 40 circuits are designed by experienced analog engineers under commercial 180nm technology, covering various functional types, including operational transconductance amplifier (OTA), comparator (COMP), bandgap reference circuit, low dropout regulator circuit (LDO) and oscillator circuit, which are widely used in analog front-end applications. The OTA circuit is commonly employed as a signal-processing component. The COMP circuit facilitates comparison between analog and reference signals, subsequently generating digital signals or switching control signals based on the comparison results. The COMP circuit is valued for its high speed, accuracy, and common mode rejection ratio (CMRR), and its device parameters significantly impact the performance of the entire circuit. A bandgap reference circuit is designed to provide PVT (process, supply voltage, temperature) insensitive reference voltages, which is a critical component in analog circuit design. The LDO circuit is a linear regulator that controls high voltage to a stable lower voltage. The low dropout characteristic makes LDO circuits useful in applications that require high output voltage accuracy, a wide range of input voltage, and low power consumption, such as mobile devices, wireless communication, and embedded systems. The oscillator circuit is used to generate periodic electrical signals, such as sine waves, square waves, pulses, etc. These electrical signals are commonly employed as clock signals, frequency references, modulation/demodulation, communication systems, and timing control in various electronic devices.

Based on these 40 circuits, two datasets are constructed, the first of which contains all circuits named Hybrid, while the second includes only the OTA circuits denoted OTA. As described in Section III-A, the SPICE circuit netlist can be represented as a directed graph, where devices and IO ports are nodes, and the nets are recognized as edges. In order to avoid a match between the nodes of the different kinds of circuits, a separate graph for each circuit is constructed to form the training set. Note that we only label symmetrical devices within each circuit graph as valid device pairs. In our dataset, we define a valid pair as one that matches the type rule. Besides, for devices with extra pins (e.g., triple-well devices), we also require that the corresponding valid pair should have the same potential. We roughly divide each dataset into training and testing sets in a 3:1 ratio at the circuit level. The graph learning-based model is trained only on the training set. This ensures that the tested circuits are totally unseen to the network model, eliminating the possibility of information leaking from the testing set to the training set. Notably, the training time of the proposed EGAT model on the Hybrid and OTA datasets is only 128.211s and 57.596s respectively, indicating a very rapid training process.

¹<https://github.com/wanglijie1999/Analog-EGAT-SymExtract>

TABLE II Statistics of the datasets.

Dataset	#Graphs	#Nodes	#Edges	#Valid pairs	#Matched pairs
Hybrid	40	1378	10824	6020	821
OTA	15	552	3512	3153	358

In addition, the testing set of the Hybrid dataset encompasses all types of circuits. The statistics on the circuit graphs are listed in TABLE II.

C. Baselines Description

To verify the superiority of the proposed framework, we compare our framework with three state-of-the-art symmetric constraint detection methods, including SFA [1], ASPDAC'21 [21] and DAC'21 [23]. The SFA [1] abstracts the SPICE file into a graph representation. Following this, seed pattern detection is employed to examine the connection relationships and device attributes between the pairs of devices for matching. This process yields seed symmetric pairs, which serve as a starting point for traversing the graph to identify the remaining symmetric pairs. In ASPDAC'21 [21], a GraphSAGE model is exploited to aggregate adjacent information into node embeddings, which are adopted to identify whether two nodes are symmetric. Besides, the DAC'21 [23] presents a graph learning-based framework leveraging unsupervised learning to recognize circuit matching structures.

D. Comparison with Baselines

We compare our framework with SFA [1], ASPDAC'21 [21] and DAC'21 [23] on the two datasets. In the experiment, we distinguish the EGAT model without and with post-processing rules as "EGAT(w/o. PP)" and "EGAT", respectively. To ensure a fair comparison, all the parameters of the SOTA works are set the same as those in these original papers. TABLE III lists the experimental results. The evaluation metrics TPR, FPR, PPV, ACC, and F_1 -score are defined in Section II-C. Meanwhile, column "Inference time" denotes the average inference time on each tested circuit, which also contains the post-processing time. We emphasize the better results in bold. As shown in the table, the proposed framework significantly outperforms SFA [1], ASPDAC'21 [21] and DAC'21 [23] in almost all metrics. For example, compared with DAC'21 [23], the proposed EGAT improves the TPR, PPV, ACC, and F_1 -score by 50.26%, 15.02%, 6.48%, and 37.41%, respectively, while the FPR is reduced by 0.85% on the Hybrid dataset. Meanwhile, on the OTA dataset, the proposed EGAT framework achieves 99.58% ACC and 98.07% F_1 -score. The reason is that in SFA [1] and ASPDAC'21 [21], a limitation is imposed wherein each device can have at most one symmetry constraint. For instance, if devices v_1 and v_2 are a symmetric pair, v_1 and v_3 will never be symmetric. This limitation leads to a degradation of performance metrics, which is also why these works get a lower FPR. Besides, DAC'21 [23] does not account for devices other than MOSFETs and passive devices. Hence, the performance of DAC'21 is poor in our datasets, which

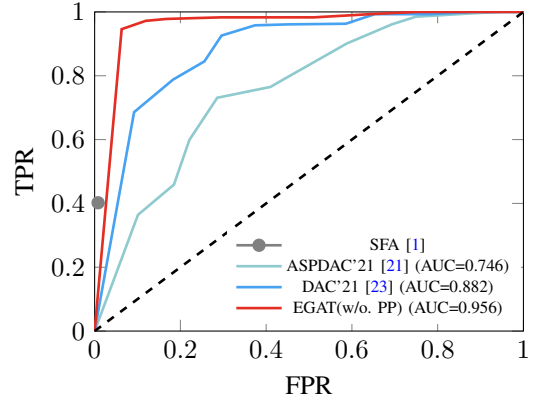


Fig. 7 The ROC curves of different models (Hybrid dataset).

also contain NPN and PNP devices. In contrast, our proposed EGAT model effectively addresses these limitations, resulting in improved performance metrics. Note that the threshold used in Equation (11) to calculate the similarity score significantly impacts the final results. TABLE IV provides the TPR and FPR values of EGAT(w/o. PP) under different thresholds. It can be observed that although higher thresholds result in lower FPR, the TPR is further decreased. After considering the overall results of various metrics, we adopted a threshold of 0.6 in the experiment. In addition, despite the higher FPR of EGAT(w/o. PP) in TABLE III, our post-processing rules can eventually reduce the final FPR.

We also evaluate the inference time of the proposed methodology. Except for SFA [1], which is compiled in C++ and exhibits faster execution time, the inference time of our EGAT model is less than those of ASPDAC'21 [21] and DAC'21 [23]. That is because our graph construction is simpler compared to ASPDAC'21 [21] and DAC'21 [23], especially for devices with a large number of pin connections. Consequently, the reduced parameters decrease the inference time.

To further demonstrate the performance of the proposed methodology, we plot the Receiver Operating Characteristic (ROC) curves of our EGAT(w/o. PP) model and the three baselines on the Hybrid dataset, respectively. For the binary classification problem, the ROC curve [37] is a graphical evaluation tool showing the FPR on the x -axis and the TPR on the y -axis. By calculating the Area Under the ROC Curve (AUC), the model's performance at different classification thresholds can be estimated. As depicted in Fig. 7, the solid gray circle represents SFA [1]. Due to the threshold-independent nature of SFA, it does not allow for adjusting thresholds. Thus, only one point on the ROC curve for SFA. The green and blue curves correspond to the ROC curves of ASPDAC'21 [21], and DAC'21 [23], with associated AUC values of 0.746 and 0.882, respectively. Meanwhile, the red curve represents the ROC curve of our EGAT(w/o. PP) model, achieving a high AUC value of 0.956. Besides, the black dashed line denotes the baseline with an AUC value of 0.5, similar to the randomized guessing. In practice, models achieving an AUC greater than 0.8 are commonly regarded as

TABLE III Comparison with state of the arts on Hybrid and OTA datasets (time unit: s).

Dataset	Model	TPR	FPR	PPV	ACC	F ₁ -score	Inference time
Hybrid	SFA [1]	0.4023	0.0081	0.8607	0.9267	0.5483	0.0389
	ASPDAC'21 [21]	0.2958	0.0022	0.9433	0.9202	0.4504	0.0799
	DAC'21 [23]	0.4437	0.0139	0.7979	0.9260	0.5703	0.0574
	EGAT(w/o. PP)	0.9463	0.0628	0.7289	0.9384	0.8048	0.0477
	EGAT	0.9463	0.0054	0.9481	0.9908	0.9444	0.0559
OTA	SFA [1]	0.3750	0.0091	0.8295	0.9257	0.5163	0.0296
	ASPDAC'21 [21]	0.2682	0.0013	0.9642	0.9135	0.4196	0.1136
	DAC'21 [23]	0.3600	0.0218	0.7500	0.8833	0.4865	0.0993
	EGAT(w/o. PP)	1.0000	0.0206	0.8502	0.9815	0.9166	0.0758
	EGAT	1.0000	0.0047	0.9629	0.9958	0.9807	0.0941

TABLE IV The FPR and TPR values of EGAT(w/o. PP) at different thresholds (Hybrid dataset).

Threshold	0.5	0.6	0.7	0.8	0.9	0.99
FPR	0.0908	0.0628	0.0450	0.0365	0.0214	0.0070
TPR	0.9565	0.9463	0.9318	0.9018	0.8571	0.3014

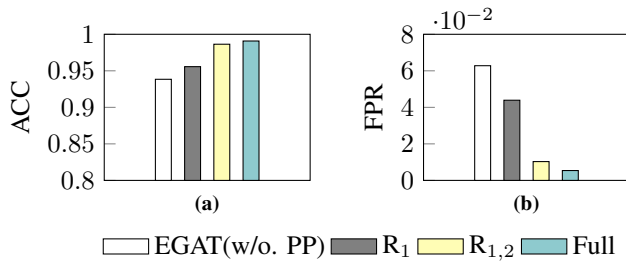


Fig. 8 Comparisons of (a) ACC and (b) FPR of different post-processing rules (Hybrid dataset).

having commendable performance, while those exceeding 0.9 are deemed excellent classifiers. Therefore, our EGAT model demonstrates outstanding classification capabilities.

In the layout automation of analog circuits, constraint extraction is the first stage where higher TPR and lower FPR values can alleviate the difficulties and computational costs of the subsequent placement and routing, significantly reducing the overall design complexity. More importantly, since the circuits vary considerably in Hybrid and OTA datasets, the experimental results also demonstrate that our framework can generalize to different types of analog circuits.

E. Ablation Study

An ablation study is performed to investigate how different post-processing rules affect the performance. Fig. 8 summarizes the contribution of the post-processing rules. “EGAT(w/o. PP)” represents the framework without any post-processing rules, “R₁” refers to the framework only with the device position rule, “R_{1,2}” stands for the framework with the device position and size rules, while “Full” is our framework with entire post-processing rules. The histogram shows that comparing the framework with only EGAT model, the post-

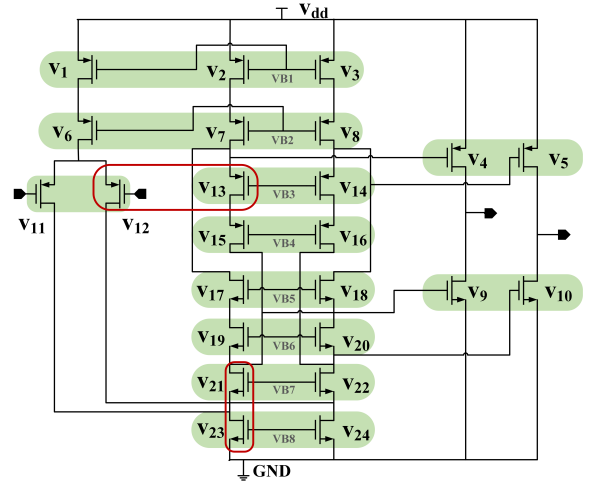


Fig. 9 Inference for a Class-AB OTA circuit.

TABLE V Comparison with the traditional GAT model on Hybrid dataset.

	TPR	FPR	PPV	ACC	F ₁ -score
GAT	0.8875	0.0926	0.5434	0.9051	0.6741
EGAT(w/o. PP)	0.9463	0.0628	0.7289	0.9384	0.8048
Improvement	+5.88%	-2.98%	+18.55%	+3.33%	+13.07%

processing rules get 5.24% further improvement on ACC and reduce 5.74% of the FPR. Fig. 9 illustrates the possible inference process for a Class-AB OTA circuit, with the green color representing symmetric pairs correctly identified by the network, and the red lines indicating asymmetric pairs incorrectly recognized by the network but removed during post-processing.

We also compare the proposed EGAT(w/o. PP) model with the traditional GAT model. In the experiment, both models utilize three graph attentional layers with nearly identical number of parameters. TABLE V lists the experimental results. It can be seen that compared to the traditional GAT model, the proposed EGAT(w/o. PP) model exhibits significant improvements in TPR, PPV, ACC, and F₁-score by 5.88%, 18.55%, 3.33%, and 13.07%, respectively, while the FPR is decreased

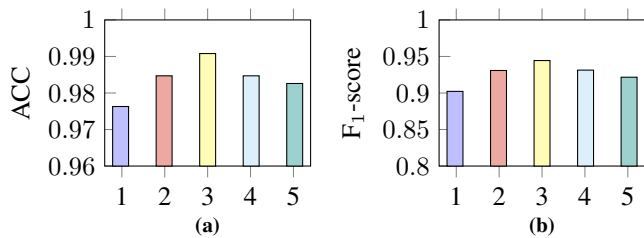


Fig. 10 Comparisons of (a) ACC and (b) F_1 -score of different layer numbers of the EGAT model (Hybrid dataset).

TABLE VI Comparison of our framework with and without the 4-dimensional gate connectivity feature (Hybrid dataset).

	TPR	FPR	PPV	ACC	F_1 -score
w/o. GF	0.9172	0.0196	0.9327	0.9827	0.9086
Full	0.9463	0.0054	0.9481	0.9908	0.9444
Improvement	+2.91%	-1.42%	+1.54%	+0.81%	+3.58%

by 2.98%. The reason is that the GAT model only focuses on node-level features and cannot achieve feature interaction between nodes and edges. As a consequence, suboptimal predictions are produced with more non-matching pairs being incorrectly identified as matching pairs.

Another ablation study is performed on the graph learning framework to investigate how the number of network layers in the EGAT model affects the performance. Fig. 10 depicts the changes of ACC and F_1 -score on the Hybrid dataset with respect to the model’s layer numbers. As illustrated in the histogram, with the network depth increasing, ACC and F_1 -score get saturated and then decreases gradually. Thus, it is reasonable to set the layer numbers of the EGAT model to 3.

We further conduct a fourth ablation experiment to demonstrate the impact of the input feature on the final performance. As described in Section III-B, a 15-dimensional node feature is defined, comprising a 4-dimensional vector that describes the connection relationships among gate ports. TABLE VI records the influence of the 4-dimensional gate connectivity vector. Column “w/o. GF” refer to the model without the 4-dimensional gate feature, while “Full” is our framework with all defined features. It can be seen that by incorporating the gate port connectivity vector, the TPR, PPV, ACC, and F_1 -score are enhanced by 2.91%, 1.54%, 0.81%, and 3.58%, while the FPR is reduced by 1.42%, demonstrating the effectiveness of the defined node features.

V. CONCLUSION

In this paper, we have proposed a graph learning framework to automatically extract symmetric constraints in analog circuits, which effectively combines edge information in a graph with attentional mechanisms. Suitable circuit features are designed to guide the network model to achieve information interaction with devices. Besides, several post-processing rules are developed to significantly reduce the false positive rate. Experimental results show that, compared with the SOTA implementations, our approach produces better performance.

In the future, we will extend the framework to recognize system-level symmetries in analog circuits.

REFERENCES

- [1] B. Xu, K. Zhu, M. Liu, Y. Lin, S. Li, X. Tang, N. Sun, and D. Z. Pan, “MAGICAL: Toward fully automated analog IC layout leveraging human and machine intelligence,” in *IEEE/ACM International Conference on Computer-Aided Design (ICCAD)*, 2019, pp. 1–8.
- [2] K. Kunal, M. Madhusudan, A. K. Sharma, W. Xu, S. M. Burns, R. Harjani, J. Hu, D. A. Kirkpatrick, and S. S. Sapatnekar, “ALIGN: Open-source analog layout automation from the ground up,” in *ACM/IEEE Design Automation Conference (DAC)*, 2019, pp. 1–4.
- [3] U. Choudhury and A. Sangiovanni-Vincentelli, “Constraint generation for routing analog circuits,” in *ACM/IEEE Design Automation Conference (DAC)*, 1991, pp. 561–566.
- [4] E. Malavasi, E. Charbon, E. Felt, and A. Sangiovanni-Vincentelli, “Automation of ic layout with analog constraints,” *IEEE Transactions on Computer-Aided Design of Integrated Circuits and Systems (TCAD)*, vol. 15, no. 8, pp. 923–942, 1996.
- [5] E. Charbon, E. Malavasi, and A. Sangiovanni-Vincentelli, “Generalized constraint generation for analog circuit design,” in *IEEE/ACM International Conference on Computer-Aided Design (ICCAD)*, 1993, pp. 408–414.
- [6] S. Bhattacharya, N. Jangkrajarn, R. Hartono, and C.-J. Shi, “Hierarchical extraction and verification of symmetry constraints for analog layout automation,” in *IEEE/ACM Asia and South Pacific Design Automation Conference (ASPDAC)*. IEEE, 2004, pp. 400–405.
- [7] P.-H. Wu, M. P.-H. Lin, T.-C. Chen, C.-F. Yeh, X. Li, and T.-Y. Ho, “A novel analog physical synthesis methodology integrating existent design expertise,” *IEEE Transactions on Computer-Aided Design of Integrated Circuits and Systems (TCAD)*, vol. 34, no. 2, pp. 199–212, 2014.
- [8] P.-H. Wu, M. P.-H. Lin, and T.-Y. Ho, “Analog layout synthesis with knowledge mining,” in *European Conference on Circuit Theory and Design (ECCTD)*, 2015, pp. 1–4.
- [9] Q. Hao, S. Chen, X. Hong, Y. Su, S. Dong, and Z. Qu, “Constraints generation for analog circuits layout,” in *International Conference on Communications, Circuits and Systems (ICCCAS)*, 2004, pp. 1334–1338.
- [10] Z. Zhou, S. Dong, X. Hong, Q. Hao, and S. Chen, “Analog constraints extraction based on the signal flow analysis,” in *International Conference on ASIC (ASICON)*, 2005, pp. 825–828.
- [11] T. Massier, H. Graeb, and U. Schlichtmann, “The sizing rules method for CMOS and bipolar analog integrated circuit synthesis,” *IEEE Transactions on Computer-Aided Design of Integrated Circuits and Systems (TCAD)*, vol. 27, no. 12, pp. 2209–2222, 2008.
- [12] M. Eick, M. Strasser, K. Lu, U. Schlichtmann, and H. E. Graeb, “Comprehensive generation of hierarchical placement rules for analog integrated circuits,” *IEEE Transactions on Computer-Aided Design of Integrated Circuits and Systems (TCAD)*, vol. 30, no. 2, pp. 180–193, 2011.
- [13] M. Liu, W. Li, K. Zhu, B. Xu, Y. Lin, L. Shen, X. Tang, N. Sun, and D. Z. Pan, “ S^3 DET: Detecting system symmetry constraints for analog circuits with graph similarity,” in *IEEE/ACM Asia and South Pacific Design Automation Conference (ASPDAC)*, 2020, pp. 193–198.
- [14] L. Guo, K. Wang, and T. Wang, “Open-circuit fault diagnosis of three-phase permanent magnet machine utilizing normalized flux-producing current,” *IEEE Transactions on Industrial Electronics (TIE)*, vol. 71, no. 4, pp. 3351–3360, 2024.
- [15] T. Gao, J. Yang, S. Jiang, and Y. Li, “An incipient fault diagnosis method based on complex convolutional self-attention autoencoder for analog circuits,” *IEEE Transactions on Industrial Electronics (TIE)*, 2023.
- [16] T. Gao, J. Yang, and S. Jiang, “A novel fault detection model based on vector quantization sparse autoencoder for nonlinear complex systems,” *IEEE Transactions on Industrial Informatics (TII)*, vol. 19, no. 3, pp. 2693–2704, 2022.
- [17] T. Dhar, J. Poojary, Y. Li, K. Kunal, M. Madhusudan, A. K. Sharma, S. D. Manasi, J. Hu, R. Harjani, and S. S. Sapatnekar, “Fast and efficient constraint evaluation of analog layout using machine learning models,” in *IEEE/ACM Asia and South Pacific Design Automation Conference (ASPDAC)*, 2021, pp. 158–163.
- [18] K. Zhu, H. Chen, W. J. Turner, G. F. Kokai, P.-H. Wei, D. Z. Pan, and H. Ren, “TAG: Learning circuit spatial embedding from layouts,” in *IEEE/ACM International Conference on Computer-Aided Design (ICCAD)*, 2022, pp. 1–9.

- [19] K. Hakhamaneshi, M. Nassar, M. Phielipp, P. Abbeel, and V. Stojanovic, "Pretraining graph neural networks for few-shot analog circuit modeling and design," *IEEE Transactions on Computer-Aided Design of Integrated Circuits and Systems (TCAD)*, vol. 42, no. 7, pp. 2163–2173, 2023.
- [20] K. Kunal, J. Poojary, T. Dhar, M. Madhusudan, R. Harjani, and S. S. Sapatnekar, "A general approach for identifying hierarchical symmetry constraints for analog circuit layout," in *IEEE/ACM International Conference on Computer-Aided Design (ICCAD)*, 2020, pp. 1–8.
- [21] X. Gao, C. Deng, M. Liu, Z. Zhang, D. Z. Pan, and Y. Lin, "Layout symmetry annotation for analog circuits with graph neural networks," in *IEEE/ACM Asia and South Pacific Design Automation Conference (ASPDAC)*, 2021, pp. 152–157.
- [22] W. Hamilton, Z. Ying, and J. Leskovec, "Inductive representation learning on large graphs," in *Conference on Neural Information Processing Systems (NIPS)*, 2017, pp. 1025–1035.
- [23] H. Chen, K. Zhu, M. Liu, X. Tang, N. Sun, and D. Z. Pan, "Universal symmetry constraint extraction for analog and mixed-signal circuits with graph neural networks," in *ACM/IEEE Design Automation Conference (DAC)*, 2021, pp. 1243–1248.
- [24] K. Zhu, H. Chen, M. Liu, and D. Z. Pan, "Automating analog constraint extraction: From heuristics to learning," in *IEEE/ACM Asia and South Pacific Design Automation Conference (ASPDAC)*, 2022, pp. 108–113.
- [25] K. Kunal, T. Dhar, M. Madhusudan, J. Poojary, A. K. Sharma, W. Xu, S. M. Burns, J. Hu, R. Harjani, and S. S. Sapatnekar, "GNN-based hierarchical annotation for analog circuits," *IEEE Transactions on Computer-Aided Design of Integrated Circuits and Systems (TCAD)*, vol. 42, no. 9, pp. 2801–2814, 2023.
- [26] W. Yao, X. Gao, Y. Lin, and L. Li, "Automatic layout symmetry extraction for analog constraint learning," in *International Symposium of Electronics Design Automation (ISED)*, 2023, pp. 76–81.
- [27] T. N. Kipf and M. Welling, "Semi-supervised classification with graph convolutional networks," *arXiv preprint arXiv:1609.02907*, 2016.
- [28] M. Simonovsky and N. Komodakis, "GraphVAE: Towards generation of small graphs using variational autoencoders," in *International Conference on Artificial Neural Networks (ICANN)*, 2018, pp. 412–422.
- [29] A. Vaswani, N. Shazeer, N. Parmar, J. Uszkoreit, L. Jones, A. N. Gomez, L. Kaiser, and I. Polosukhin, "Attention is all you need," in *Conference on Neural Information Processing Systems (NIPS)*, 2017, pp. 1–11.
- [30] P. Veličković, G. Cucurull, A. Casanova, A. Romero, P. Lio, and Y. Bengio, "Graph attention networks," *arXiv preprint arXiv:1710.10903*, 2017.
- [31] M. S. Hussain, M. J. Zaki, and D. Subramanian, "Global self-attention as a replacement for graph convolution," in *ACM International Conference on Knowledge Discovery and Data Mining (KDD)*, 2022, pp. 655–665.
- [32] J. L. Ba, J. R. Kiros, and G. E. Hinton, "Layer normalization," *arXiv preprint arXiv:1607.06450*, 2016.
- [33] K. He, X. Zhang, S. Ren, and J. Sun, "Deep residual learning for image recognition," in *IEEE Conference on Computer Vision and Pattern Recognition (CVPR)*, 2016, pp. 770–778.
- [34] C. M. Bishop and N. M. Nasrabadi, *Pattern recognition and machine learning*. Springer, 2006, vol. 4, no. 4.
- [35] A. Paszke, S. Gross, S. Chintala, G. Chanan, E. Yang, Z. DeVito, Z. Lin, A. Desmaison, L. Antiga, and A. Lerer, "Automatic differentiation in PyTorch," in *NIPS Workshop*, 2017.
- [36] D. P. Kingma and J. Ba, "Adam: a method for stochastic optimization," *arXiv preprint arXiv:1412.6980*, 2014.
- [37] John, A., and Swets, "The relative operating characteristic in psychology," *Science*, 1973.